DYNAMIC PROPERTIES OF ELECTROTONIC COUPLING BETWEEN CELLS OF EARLY *XENOPUS* EMBRYOS

R. A. DiCAPRIO, A. S. FRENCH, *and* E. J. SANDERS

From the Department of Physiology, University of Alberta, Edmonton, Alberta, Canada

ABSTRACT Frequency response functions were measured between the cells of *Xenopus laevis* embryos during the first two cleavage stages. Linear systems theory was then used to produce electronic models which account for the electrical behavior of the systems. Coupling between the cells may be explained by models which have simple resistive elements joining each cell to its neighbors. The vitelline, or fertilization, membrane which surrounds the embryos has no detectable resistance to the passage of electric current. The electrical properties of the four-cell embryo can only be explained by the existence of individual junctions linking each pair of cells. This arrangement suggests that electrotonic coupling is important in the development of the embryos, at least until the four-cell stage.

INTRODUCTION

It is well established that many cells are capable of exchanging ions and small molecules by means of low resistance intercellular junctions (for reviews see Furshpan and Potter, 1968; Loewenstein, 1966, 1967). Ultrastructural investigations in a number of cell types have indicated that the low resistance junctions mediating this intercellular communication or coupling may be closely correlated with septate junctions or with gap junctions (Loewenstein, 1966; Payton et al., 1969; McNutt and Weinstein, 1970; Rose, 1971). There has been considerable speculation on the functional implications of such junctions during development (for example Loewenstein, 1966, 1968 *a*, *b*) where the transfer of materials between cells could be a factor in controlling the growth, division, and differentiation of the cells in the system, and for this reason there have been studies on coupling between cells in a variety of invertebrate and vertebrate embryos: molluscs (Potter et al., 1966; Furshpan and Potter, 1968), echinoderms (Ashman et al., 1964; Tupper et al., 1970; Tupper and Saunders, 1972), teleosts (Bennett and Trinkhaus, 1970; Bennett et al., 1972; Bozhkova et al., 1971), amphibians (Ito and Hori, 1966; Takahashi and Ito, 1968; Ito and Loewenstein, 1969; Palmer and Slack, 1970; Slack and Palmer, 1969; Sheridan, 1971), and birds (Sheridan, 1968).

We have examined the electrical characteristics of the plasma memdranes anb intercellular coupling between all of the cells in the first two cleavage stages of *Xenopus laevis* embryos. Electrical models of these cell systems have been constructed taking into account the resistive and capacitive properties of the plasma (nonjunctional) membranes, the junctional membranes and the vitelline, or fertilization membrane. Data is available on the ultrastructure of cell contacts at these stages of *Xenopus* development (Sanders and Zalik, 1972; Singal and Sanders, 1974) allowing speculation on some aspects of the mechanism of intercellular coupling in this system by a correlation of electrophysiological and morphological findings.

Earlier electrical studies of embryonic systems have concentrated on measurements of coupling ratios between cells, where coupling ratio is defined as the ratio of the voltage changes in two coupled cells when one cell is subjected to electrical stimulation. Other parameters which have been studied repeatedly are the resting membrane potentials of the cells and their apparent cell membrane resistance. However, if the coupling ratio between two cells is greater than zero, then neither of these measurements define primary membrane characteristics since they reflect the lumped properties of junctional and nonjunctional membranes of a number of cells. Another feature of previous work on these systems is that it has concerned itself primarily with the direct current, or resistive properties of the membranes. Although some cell input time constants have been estimated by measuring the rise times of cell membrane potentials when subjected to rectangular current pulses (Bennett et al., 1972), no attempts have been made to accurately measure junctional or nonjunctional membrane capacitances.

All previous studies on electrically coupled embryonic systems have indicated that they may be modeled by simple linear electrical networks consisting entirely of resistances and capacitances. The relationship between the voltages, as functions of time, at any two nodes, or points of connection, in such a network may be completely characterized in terms of the individual components and in either the time or frequency domains. The rediscovery by Cooley and Tukey (1965) of the fast Fourier transform, has made analysis in the frequency domain the most efficient means of characterizing linear systems.

The voltages, $V_a(f)$ and $V_b(f)$, at two nodes are related by:

$$V_b(f) = V_a(f)H_{ab}(f), \tag{1}$$

where $H_{ab}(f)$ is the frequency response function relating the two nodes, a and b, nodes, a and b, and f is frequency. $H_{ab}(f)$ is normally a complex function but may be separated into two real functions:

$$G_{ab}(f) = |H_{ab}(f)| \tag{2}$$

$$P_{ab}(f) = \arctan H_{ab}(f), \tag{3}$$

where $G_{ab}(f)$ and $P_{ab}(f)$ are the gain and phase portions of the frequency response function, respectively.

The meaning of the frequency response function may be most easily understood in terms of sinusoidal stimulation experiments, which were the classical means of obtaining the measurement. If sinusoidal stimulation is applied to one node of the network, then the voltages observed at all other nodes will also be sinusoids, of the same frequency as the stimulation, but differing in relative amplitude and relative phase to the input. The frequency response function between two nodes measures the ratio of the two amplitudes, $G_{ab}(f)$, and the differences of the two phase shifts relative to the input sinusoid, $P_{ab}(f)$. The frequency response function may thus be measured by stimulating the system with a range of sinusoidal frequencies, f, but this is a relatively inefficient technique and has the disadvantage of requiring many time-consuming measurements. A more satisfactory approach is to stimulate the system with a white noise voltage signal. White noise may be considered to consist of a wide range of sinusoidal components with a random distribution of amplitudes and phase relationships, and the frequency response function between two codes may be obtained by measuring the resultant noise signals at the nodes, and correlating them in the frequency domain (Wiener, 1930).

A given linear electrical network will have completely predictable frequency response functions between the nodes, or points of component interconnection. The converse relationship does not necessarily hold since it is impossible to distinguish electrically between a simple element and two or more parallel simple elements of the same type. Thus for example, it is impossible to decide whether a resistance is, in reality, a group of parallel resistances. However, if the frequency response functions between all of the nodes are known, then it is possible to compute the minimum network of simple elements which will explain the behavior.

The analysis problem for an electrotonically coupled biological system is therefore twofold: to determine the locations of the nodes in the network, and to separate parallel, similar elements by arguments based on data separate from the electrical measurements. Our approach to these problems is to commence with the simplest possible networks, based on current understanding of the systems, and to add components to the network only when necessary to explain the electrical behavior of the system, as characterized by the frequency response functions, and when such components are morphologically plausible.

MATERIALS AND METHODS

Preparation of Embryos

Fertilized ova were obtained by injection of adult *Xenopus laevis* with Antuitrin-S (Parke, Davis & Co., Detroit, Mich.). Females and males received 1,000 and 500 IU of the hormone, respectively. Embryos were handled in Steinberg's Physiological Salt Solution (Hamburger, 1960) and were partially de-jellied in a solution of papain-cysteine hydrochloride for 2 min

at room temperature (Dawid, 1965). Care was taken to prevent complete removal of the jelly in order to preclude damage to the vitelline membrane and the embryos were washed in fresh saline at least six times to remove traces of the enzyme mixture. Residual jelly was removed with forceps just prior to each experiment.

Electrical Measurements

The basic experimental arrangement is illustrated diagramatically in Fig. 1. Embryos were placed in a small depression in a layer of paraffin wax at the base of a shallow dish filled with Steinberg's solution. This arrangement allowed repeated location of embryos in the same position relative to the microscope and electrodes, as well as preventing lateral movement during impalement. Glass microelectrodes were filled with 3 M KCl solution and had resistances in the range 3–5 $\times$ 10^6 Ω. Three microelectrodes were used in each experiment, two for intracellular recording and one for intracellular current injection. All electrodes were connected to the electronic apparatus via Ag/AgCl junctions, and the saline medium was connected to electrical ground via a 3 M KCl/agar bridge and an Ag/AgCl junction. Intracellular voltages were observed using bridge electrometers having resistance and capacitance compensation (M4-RM; W-P Instruments, Inc., Hamden, Conn.). Electrical sine wave stimulation was obtained from a function generator (3300A; Hewlett-Packard Co., Palo Alto, Calif.) and white noise stimulation was obtained from a generator designed to produce an even power distribution in the frequency range 1–400 Hz (French, 1973*a*). Stimulating signals passed through a fixed resistance of 10^8 Ω before entering the microelectrode, to allow current measurement independent of the electrode resistance. The maximum range of intracellular voltage displacement was ±15 mV. Intracellular voltages and the voltage proportional to the injected current were recorded on an FM tape recorder (T3000; Thermionics Products Co., Plainfield, NJ.) for subsequent processing on a LAB-8 computer. When necessary, signals were recorded at the time of the experiment on a multichannel paper chart recorder (R411; Beckman Instruments, Inc., Fullerton, Calif.).

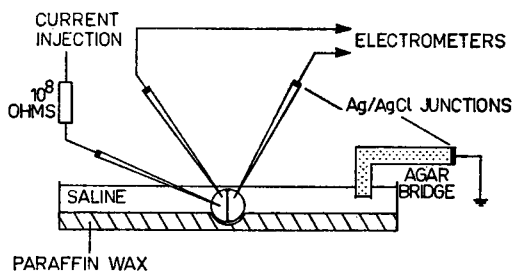

FIGURE 1

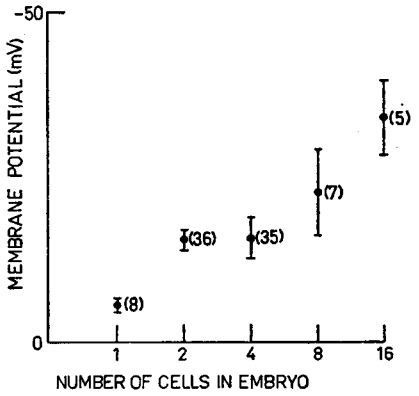

FIGURE 2

FIGURE 1 Basic experimental arrangement for the injection of current into one cell of an embryo while recording the voltages in the injected and adjacent cells.

FIGURE 2 Recorded membrane potentials for embryos at different cleavage stages. The upper and lower limits on each measurement are the standard deviations, and the figures in parentheses next to each result are the total number of observations used.

Frequency Domain Analysis

Frequency response functions were estimated by the use of a software package designed for the LAB-8 computer. The package processes two continuous time domain signals which are assumed to be the input and output signals of the system under investigation. The final products of the programs are estimates of the input power spectrum, $S_{aa}(f)$, output power spectrum, $S_{bb}(f)$, and the cross spectrum, $S_{ab}(f)$ (French and Holden, 1971; French, 1973 *b*). The cross spectrum is normally complex and is separated into real and imaginary values. The frequency response function of the system is then calculated from:

$$G_{ab}(f) = |S_{ab}(f)|/S_{aa}(f) \quad (4)$$

$$P_{ab}(f) = \arctan S_{ab}(f). \quad (5)$$

From the spectral estimates it is also possible to compute the coherence function, $\gamma^2_{ab}(f)$, of the system from:

$$\gamma^2_{ab}(f) = |S_{ab}(f)|^2/S_{aa}(f)S_{bb}(f). \quad (6)$$

The coherence function is a normalized measure of the extent to which the linear frequency response function characterizes the input-output relations of the system (Bendat and Piersol, 1966). Coherence may vary over the range $0 \leq \gamma^2 \leq 1$ and a linear, noise-free system would have a coherence of unity at all frequencies.

Each of our experiments resulted in three voltage records consisting of: (*a*) the input signal, (*b*) the voltage in the cell subjected to current injection, and (*c*) the voltage in a coupled cell. Each set of data was thus processed twice, using the first and second and then second and third signals as the input and output. In this manner two frequency response functions were obtained from each experiment, corresponding to the voltage relationships across the fixed input resistance and the junction between the two cells, respectively.

Frequency response functions are displayed in the form of Bode plots (D'Azzo and Houpis, 1966) which consist of the gain, in decibels, and the phase, in degrees, plotted versus the logarithm of the frequency. The coherence function is also plotted with each Bode plot against the same frequency axis.

Electrical Modeling

The behavior of electrical models of embryo membrane systems was evaluated by the use of a computer simulation program (IBM Application Program GH 20-0170-2, Electronic Circuit Analysis Program [ECAP]) using the University of Alberta IBM 360/67 computer. This program allows the user to simulate a network consisting of standard electronic components and describe the electrical behavior of the network by obtaining the voltages at all the nodes of the network when a voltage source is connected between two nodes. If the voltage source is sinusoidal the frequency response may be obtained by comparing the resultant sinusoids at each node.

Microscopy

Preparative procedures for electron microscopy were carried out as described previously (Sanders and Zalik, 1972). Sections at 2 μm thickness were taken for light microscopy from glutaraldehyde fixed and araldite embedded material and were stained with a mixture of equal volumes of 1% methylene blue and 1% azure B in 0.5% borax solution.

RESULTS

Membrane Penetration, Potentials, and Sealing

The successful penetration of recording microelectrodes into the embryonic cells was monitored by the detection of intracellular membrane potentials. Membrane potentials were measured as an aid in establishing the correct stage of the embryo and for comparison with previous measurements in early *Xenopus* embryos (Palmer and Slack, 1970; de Laat et al., 1973). Fig. 2 illustrates a summary of our membrane potential data for a total of 91 embryos from the 1- to 16-cell stage.

Penetration of the current injecting electrode into a cell was monitored by connecting a slow (0.5 Hz) sinusoidal stimulating signal of 5 V peak-to-peak amplitude to the electrode before impalement and observing a sinusoidal modulation in the two recorded membrane potentials.

Following membrane penetration, a sealing process occurred in the membrane surrounding the electrode. Sealing was accompanied by an increase in apparent membrane resistance and by the formation of a heavily pigmented ring around the point of electrode entry. This sealing reaction has been described previously in *Xenopus* embryos and in other tissues (Palmer and Slack, 1970; Bluemink, 1972; de Laat et al., 1973; Oliveira-Castro and Loewenstein, 1971). The process, as measured by the change in membrane resistance, was relatively slow, taking a minimum of 5 min before further change was undetectable. Fig. 3 illustrates the beginning of an experiment in which the input resistance was monitored by injecting a slow sinusoidal current of constant amplitude while measuring the modulation in membrane potential.

In all of our experiments complete membrane sealing, as indicated by stabilization of the input resistance, was allowed to proceed before further measurements were made.

Electrical Properties of the Vitelline Membrane

Previously reported electrical investigation of *Xenopus* embryos have been conducted with the external vitelline, or fertilization, membrane intact. However, if the vitelline membrane possesses resistance and capacitance comparable to the plasma membrane within it, then there will be a profound effect upon the measured plasma membrane characteristics. Electrical coupling measurements will also be affected because an embryo having a similar vitelline membrane resistance to cell membrane resistances would appear to possess electrotonic coupling between the cells when the coupling is measured relative to the external solution. This apparent coupling would occur even though there might not be any membrane specializations acting to reduce the normal intercellular resistance. Ito and Loewenstein (1969) have described a similar situation in *Triturus* embryos, where disruption of the morula surface leads to a reduction in the apparent intercellular coupling. In view of this

possible interference by the vitelline membrane we used two methods of measuring its electrical properties.

Direct measurement of vitelline characteristics was possible by placing electrode tips in the perivitelline space. Such an experiment was most easily conducted in the region directly adjacent to the cleavage furrows, where the space was most pronounced. Fig. 4 illustrates an experiment in which the current injecting electrode was placed in one cell of a two-cell embryo while a recording electrode was placed in the adjacent cell. A second recording electrode was then advanced through the vitelline membrane into the perivitelline space. Although a small membrane potential was observed in the perivitelline space, no sinusoidal modulation due to the injected current could be detected. This was interpreted as meaning that the value of the vitelline membrane resistance was smaller than could be detected by our measuring technique, and at least several powers of 10 smaller than the plasma cell membrane resistance.

Indirect evidence of the electrical properties of the vitelline membrane was ob-

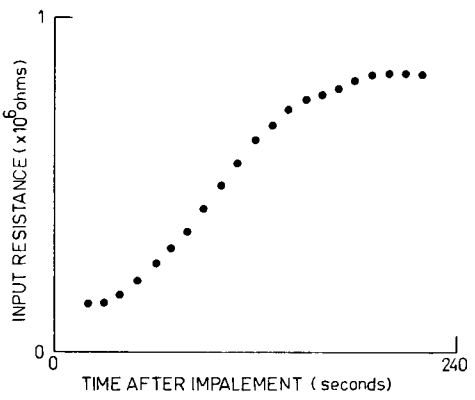

FIGURE 3

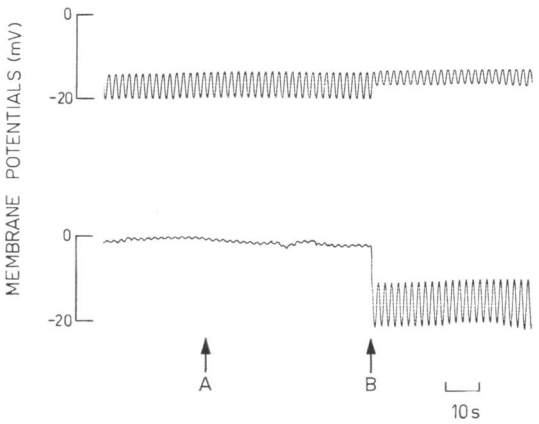

FIGURE 4

FIGURE 3 The change in cellular input resistance accompanying membrane sealing which follows penetration with a microelectrode. This sealing reaction is also indicated by the formation of a heavily pigmented ring around the electrode.

FIGURE 4 Demonstration of vitelline membrane electrical properties. A microelectrode has been inserted into one cell of a two-cell embryo and is injecting sinusoidal current. A second electrode has been placed in the adjacent cell and is recording the coupled modulation (upper trace). A third electrode is positioned just outside the embryo in the saline medium and is recording some unavoidable pickup of the stimulating voltage (lower trace). At time *A*, the third electrode is pushed through the vitelline membrane into the perivitelline space and records a small negative membrane potential, but no increase in sinusoidal modulation. At time *B*, the electrode is pushed further into the embryo and through the first cell membrane, at which point a normal membrane potential with a large sinusoidal modulation is observed. At the same time, the physical movement causes the electrode in the adjacent cell to become somewhat unsealed and its modulation level decreases. The absence of modulation in the vitelline membrane potential is interpreted to mean that it has very low resistance.

tained during experiments with white noise stimulation. On several occasions the frequency response characteristics of embryonic cells were measured, initially with the vitelline membrane intact, and then again for the same embryo after careful surgical removal of the membrane. Although it was extremely difficult to remove the membrane without causing some change in the apparent membrane resistance, presumably by damage to the plasma membrane, in eight experiments there were three occasions on which embryonic cells had identical electrical properties before and after vitelline membrane removal.

Electron microscopical observation of the embryo cortex (Fig. 5) showed the vitelline membrane to be a bilaminar structure varying in overall width from 1.4

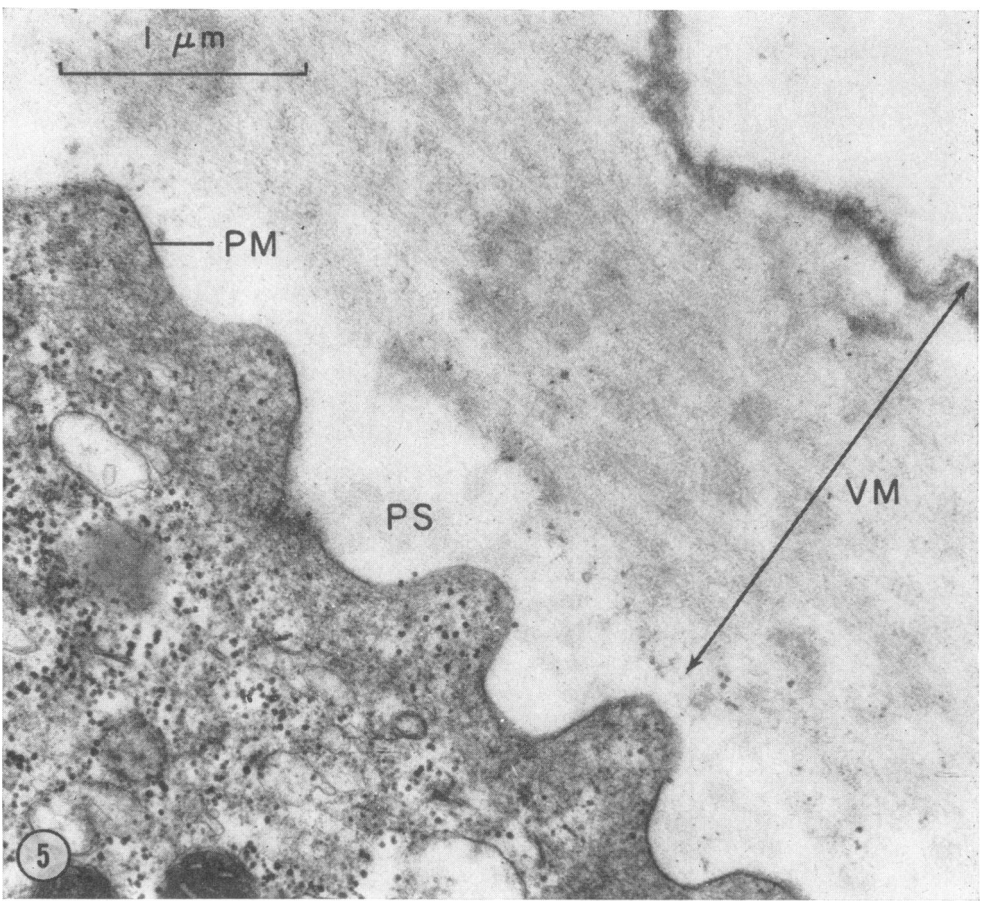

FIGURE 5 Electron micrograph of a section through the cortical region of a *Xenopus laevis* embryo showing the vitelline membrane (VM) *in situ*, the perivitelline space (PS) and the plasma membrane (PM). The width of the perivitelline space may vary according to the region of the embryo and the method of preparation for electron microscopy.

to 2.2 μm. The thin, 0.1 μm amorphous, outer lamina was more electron dense than the inner lamina which displayed a loose fibrillar structure. This diffuse structure would appear to be consistent with that expected of a membrane displaying a low ionic resistance. The extracellular layers of *Xenopus* vary in morphology from that of *Triturus* (Salthe, 1963) which has been used in some previous studies of amphibian embryonic cell coupling (Ito and Hori, 1966). In view of these indications that the vitelline membrane resistance was negligible compared with the plasma membrane resistance of the cells, we conducted our succeeding experiments with the vitelline membrane intact.

Staging of Embryos

It was not possible to judge from the external appearance alone whether a cleavage had completely divided a cell into two daughter cells. The second embryonic cleavage always started before the completion of the first, making it impossible to define a cleavage stage solely on external morphology. In categorizing embryos as two-cell or four-cell stages four separate criteria were used. Each of these criteria had to be satisfied throughout the experiment before the result was accepted as being typical of that embryonic stage. The criteria were as follows:

(*1*) External morphology of the embryo. In order to distinguish a complete two-cell embryo the data of Bluemink (1971) was used which indicates that the first cleavage is complete approximately 35 min after its initial appearance as a shallow groove. This has been confirmed by scanning electron microscopy of the internal surfaces (Sanders and Singal, 1973) which indicates that the first cleavage is complete by the time the second cleavage is a shallow groove. Four-cell embryos were not used until after the appearance of the third cleavage furrow.

(*2*) Membrane potential. As illustrated earlier, the membrane potential of the embryonic cells varies substantially with the stage. Although this is not a good criterion for the separation of two- and four-cell stages, it is useful for rejecting one- and eight-cell stages.

(*3*) Coupling ratio. This parameter can be measured immediately after the cells are penetrated and allows a clear distinction between single cells, with a coupling ratio of unity, and other embryos.

(*4*) Frequency response function. This was a retrospective selector because it was not available until after the experiment had been completed. However, a result which was clearly outside the normal limits of variation was rejected as probably having changed stage during the experiment.

Electrical Analysis of the Two-Cell Embryo

Fig. 6 illustrates the simplest electrical model of the two-cell embryo based on previous investigations of the system. Each cell in this model has membrane resistance and capacitance due solely to the plasma membrane and the properties of the cell

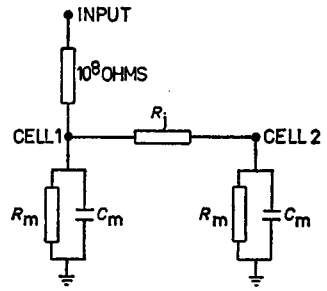

FIGURE 6 The simplest electrical model of the two-cell embryo. R_m and C_m are the cell membrane resistances and capacitances respectively while R_j is the junctional resistance. The fixed input resistance of 10^8 Ω which was used for current injection is included to allow all calculations to be made in voltage ratios.

membranes are assumed identical. The junctional coupling between the two cells is modeled by a single resistance. In order to limit the analysis entirely to voltage ratios we have included the fixed resistance, associated with the current injecting electrode, in the circuit so that the voltage used to produce the current injection is the input variable rather than the current. Using this model there are four nodes at which voltage may be measured: the input, the two cell interiors, and ground. However, we shall demonstrate that to calculate the values of the three unknown components, R_m, R_j, and C_m, of this model, it is sufficient to measure the frequency response functions between the two pairs of nodes: input-cell 1 and cell 1-cell 2.

Figs. 7 and 8 illustrate the frequency response and coherence functions between these pairs of nodes for one embryo. There was a high value of the coherence function throughout the frequency range of both these measurements (the maximum theoretical value of this function is unity). It was impossible to perform the analysis without including some extraneous variability or noise, both in the actual physical measurements and in truncation and rounding errors during the computations. Any such extraneous noise will reduce the measured coherence function as would any variability or nonlinearity internal to the system. It must be concluded from Figs. 7 and 8 that a linear model is an excellent means of accounting for the electrical behavior of the system.

A detailed account of the interpretation of a Bode plot is beyond the scope of the present paper. However, we shall attempt to give a brief introduction to the subject (an excellent discussion of Bode plot analysis is given in D'Azzo and Houpis, 1966). The low frequency asymptotes of the Bode plot must, by definition, describe the behavior of the system at zero frequency, or under steady current conditions. Since capacitances and inductances behave as infinite and zero resistances, respectively, at zero frequency, it is possible from the low frequency asymptotes to analyze the purely resistive properties of the system. If there is some noninfinite resistive path between the two nodes then the steady current:voltage ratio may be calculated from the zero frequency gain asymptote. Under these circumstances the phase curve must approach a zero frequency asymptote of 0°. The remainder of the Bode plot at non-zero frequencies is determined by all of the components in the system. There is no

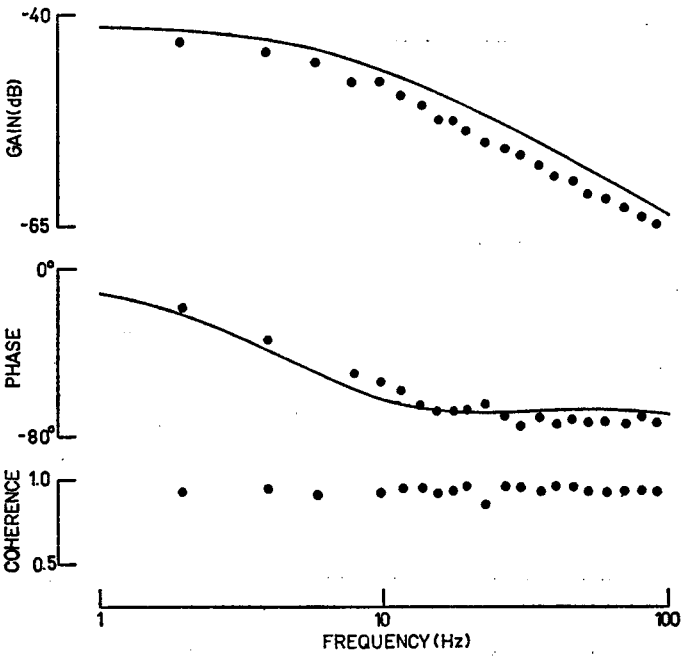

FIGURE 7 Frequency response and coherence functions between the input and cell 1 of a two-cell embryo. Filled circles are experimental results and solid lines are theoretical predictions based upon the network of Fig. 6.

evidence that significant inductive elements are present in any biological system; indeed, it is difficult to imagine any biological system which could display appreciable inductance, and so we are dealing with the combined properties of resistances and capacitances. One of the easiest ways to understand the Bode plot is in terms of time constants. The simplest example of a time constant circuit is the parallel or series combination of a single resistance and a single capacitance. A system having a single time constant will have a high frequency gain asymptote which changes by 6 dB for each doubling in frequency, or octave. At the same time the phase curve will have a high frequency asymptote of $\pm 90°$ depending on the type of system. Systems having more than one time constant have more complicated Bode plots but if the time constants are coupled in a simple manner then simple multiples of the 6 dB per octave high frequency asymptote slope are found.

From the two low frequency asymptotes of the gain curves in Figs. 7 and 8, we may measure the steady current voltage ratios : V_1/V_i and V_2/V_1, where V_i = input voltage, V_1 = voltage in cell 1, and V_2 = voltage in cell 2. Then, using the component labels from Fig. 6:

$$\frac{V_1}{V_i} = \frac{1}{1 + [10^8(R_j + 2R_m)/R_m(R_j + R_m)]}, \tag{7}$$

and

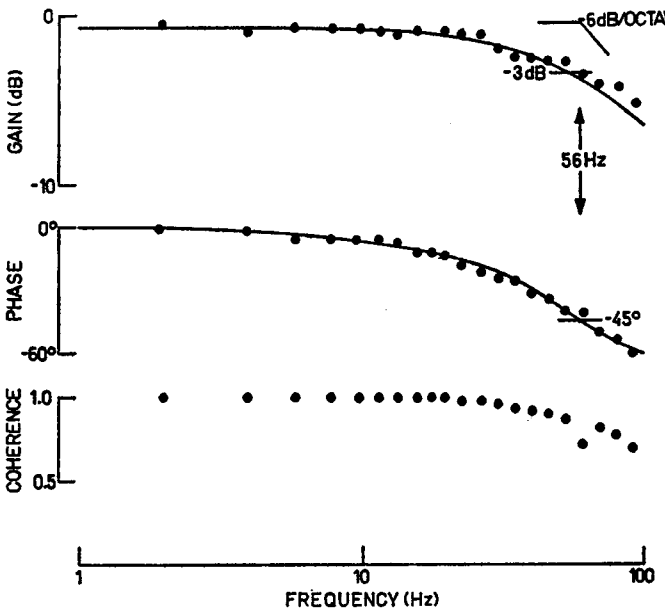

FIGURE 8 Frequency response and coherence functions between cell 1 and cell 2 of the two-cell embryo used for Fig. 7. Filled circles are experimental results and solid lines are theoretical predictions based upon the network in Fig. 6. The corner frequency, f_c, is determined by the intersection of the gain asymptotes, the passage of the phase curve through $-45°$ and the passage of the gain curve through -3 dB relative to the low frequency asymptote. In this example f_c is approximately 56 Hz.

$$\frac{V_2}{V_1} = \frac{R_m}{R_m + R_j}. \tag{8}$$

Substituting Eq. 8 into Eq. 7 allows the calculation of R_j and R_m. It should be noted that the frequently used measure of coupling ratio (CR) is, in our nomenclature, given by V_2/V_1.

Having determined the values of the membrane and junctional resistances, we may proceed to determine the membrane capacitance from either of the two available Bode plots since there is only one unknown variable. Inspection of the circuit of Fig. 6 reveals that this may be most easily accomplished by the use of the cell-to-cell measurements. In the case of the input-cell 1 frequency response function we are dealing with a system in which current flows through the fixed input resistance into two time constant circuits, given by the membrane resistances and capacitances of the two cells, but in a ratio determined by the value of the junctional resistance. This is not a simple time constant system, as is indicated by the Bode plot, Fig. 7, which, although it displays a simple gain curve in the region in which we have measured it, has a more complex phase characteristic which passes through two points of inflection. On the other hand, the frequency response function between cell 1 and

cell 2 should be simple, since in this case, whatever the voltage is in cell 1, the voltage in cell 2 should be determined from it by the simple resistive divider, $R_j - R_m$ and the single time constant of R_mC_m. Fig. 8 indicates that this is indeed the situation with the gain curve approaching a high frequency asymptote of -6 dB per octave and the phase curve approaching $-90°$.

The time constant of the R_mC_m circuit gives rise to a corner frequency in the Bode plot, above which the high frequency asymptote is approached. There are three means of determining the value of this corner frequency from the plot: (*a*) If the gain asymptotes of 0 dB per octave and -6 dB per octave, respectively, are extended towards each other, their point of intersection should be the corner frequency. (*b*) Relative to the low frequency asymptote, the gain curve should pass through a point which is 3 dB below the low frequency asymptote at the corner frequency. (*c*) The phase curve should pass through the value of $-45°$ at the corner frequency. As may be seen from Fig. 8, there is excellent agreement between these three means of measuring the corner frequency and they coincide at approximately 56 Hz.

In order to compute the membrane capacitance, C_m, from Fig. 8, we must consider the two arms of the network, cell 1-cell 2, and cell 2-ground, in terms of their complex impedances, Z_j and Z_m. Then the voltage ratio between the two cells as a function of frequency, f,

$$(V_2/V_1)\,(f) = Z_m(f)/[Z_m(f) + Z_j(f)], \tag{9}$$

where:

$$Z_m(f) = R_m/(1 + 2\pi i f C_m R_m), \tag{10}$$

$$Z_j(f) = R_j.$$

Substituting Eq. 10 and Eq. 11 into Eq. 9 gives:

$$(V_2/V_1)(f) = R_m/[R_m + R_j(1 + 2\pi i f C_m R_m)]. \tag{12}$$

This complex expression may be separated into real and imaginary parts by inverting:

$$(V_1/V_2)(f) = (1 + [R_j/R_m]) + (2\pi i f R_j C_m). \tag{13}$$

Hence the phase of V_2/V_1, defined by Eq. 1 and 3, is given by:

$$\arctan\left(-\frac{2\pi f R_j C_m}{1 + R_j/R_m}\right). \tag{14}$$

At the corner frequency, f_c, the phase passes through $-45°$ and since tan $(-45°)$ =

-1 we conclude that:

$$C_m = (1 + R_j/R_m)/2\pi f_c R_c . \quad (15)$$

Thus, knowledge of R_c, R_m, and f_c allows the calculation of C_m.

For the example of Figs. 7 and 8 the calculated values of R_m, R_j, and C_m were: 1.67×10^6 Ω, 1.46×10^5 Ω, and 0.0215 μF, respectively. These values were inserted into the modeled network of Fig. 6 and the frequency response functions for input-cell 1 and cell 1-cell 2 were calculated using the ECAP program. The resulting gain and phase curves were superimposed upon the measured characteristics and are shown as solid lines in Figs. 7 and 8. Note the excellent agreement between all four measured curves and the modeled values, including the double inflection of the Phase characteristic in Fig. 7. The circuit of Fig. 6 is thus adequate to explain the electrical behavior of the two-cell embryo over the frequency range which we have used.

Electrical Analysis of the Four-Cell Embryo

The second cleavage of the embryo results in a four-cell system with the four cells occupying approximately equal quadrants. Assuming that the cells are electrically identical there are now two possible experimental arrangements following from the two-cell experiments and which are illustrated diagramatically in Fig. 9. We may measure the voltages in two cells which are adjacent to each other when one is being stimulated, or alternatively we may measure the voltages in two diagonally opposite cells, when one is being stimulated. A model derived by simple extrapolation from the two-cell experimental results, and taking into account the four-cell geometry, would have four sets of membrane resistances and capacitances, corresponding to the four cell membranes, and four junctional resistances linking each pair of cells whose surfaces are in apposition. Electrically, this arrangement would result in two classes of cell-to-cell frequency response functions, adjacent pairs and diagonal pairs, with complex characteristics because of the two paths joining any given pair of cells, and the four membrane time constants. Models constructed using this arrangement consistently showed a diagonal cell-to-cell

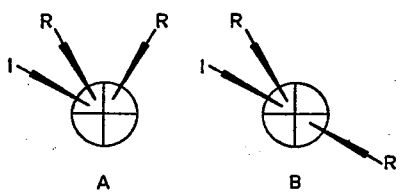

FIGURE 9 Assuming that the cells of a four-cell embryo are electrically identical, there are two possible recording arrangements: (*A*) The second recording electrode is placed in the cell adjacent to the stimulated cell. (*B*) The second electrode is placed in the cell diagonally opposite to the stimulated cell. R, recording electrode and *I*, current injecting electrode.

frequency response having a high frequency asymptote slope of −12 dB per octave. This may be understood in terms of the input signal being filtered by a membrane time constant at each of two stages before reaching the diagonal cell. However, the experimentally measured frequency responses were different from this initial prediction. Whichever pair of cells was examined, the cell-to-cell frequency response functions were not only very similar but of a simple type, having a −6 dB per octave slope in the high frequency gain asymptote and a phase characteristic having a −90° high frequency asymptote. Fig. 10 illustrates cell-to-cell frequency reponse and coherence functions for a four-cell embryo where the observed two cells were adjacent and Fig. 11 illustrates the same functions for a different embryo using diagonally opposite cells. It was technically very difficult to obtain these two measurements from the same embryo because it was impossible to decide if a cell penetrated in the first measurement had sealed completely before the second measurement. Fig. 12 illustrates the frequency response and coherence functions for the input-cell 1 system for the embryo of Fig. 11.

The simplest electrical model to explain the above results is illustrated in Fig. 13. The model has four identical sets of cell membrane components, R_m and C_m. Identical junctional resistances, R_j, are located between each pair of cells. The presence of the two diagonal junctional resistances would, initially, seem difficult to explain in terms of the morphology of the four-cell embryo, in which contact between diagonally opposed cells seems unlikely. However, we have reexamined the geometry

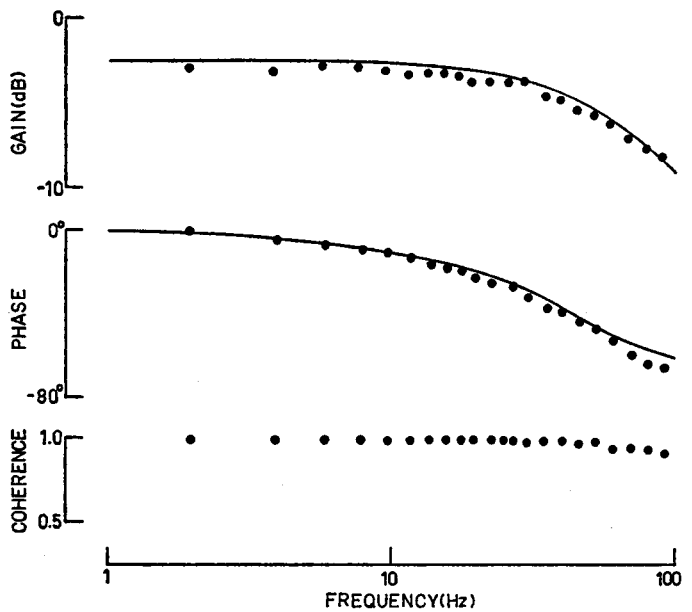

FIGURE 10 Frequency response and coherence functions between two adjacent cells in a four-cell embryo. Filled circles are experimental results and solid lines are theoretical predictions based upon the network of Fig. 13.

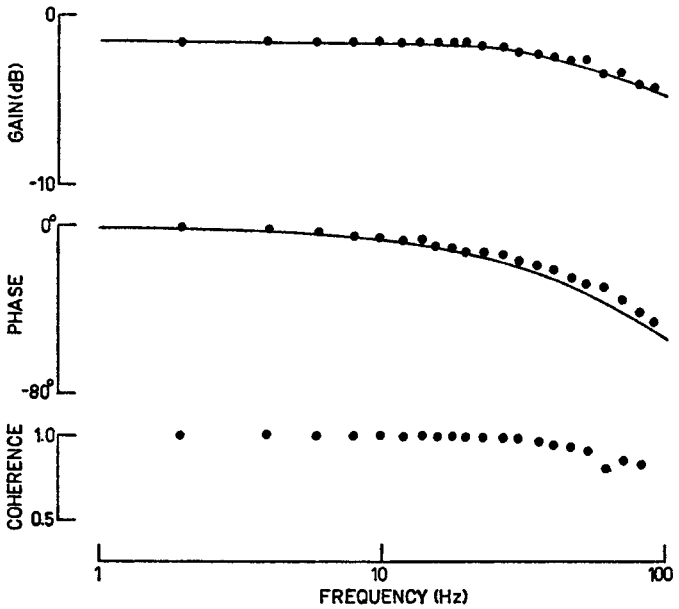

FIGURE 11 Frequency response and coherence functions between two diagonally opposed cells in a four-cell embryo. Filled circles are experimental results and solid lines are theoretical predictions based upon the network of Fig. 13. Note the very close similarity between this frequency response and that illustrated in Fig. 10 for the adjacent cells.

of these embryos and have found a morphological basis for the diagonal coupling. Fig. 14 shows a scanning electron micrograph of the animal pole of a four-cell embryo. It is clear from this figure that the geometry of the four-cell embryo is not simply one of four quadrants of a sphere, but rather there is displacement of the membranes at the poles to produce an area of contact between one pair of diagonally opposed cells, while the other pair is separated. At the vegetal pole of the embryo the situation is reversed, so that the previously separated pair of cells is now closely apposed while the other pair is parted. Fig. 15 is a section through the vegetal hemisphere of a four-cell embryo showing the close apposition of a diagonal pair of cells.

It may at first be thought that the electrical network of Fig. 13 would be more difficult to analyse than if the two diagonal coupling resistances had been absent. However, the diagonal coupling actually facilitates the analysis by producing a system with very high symmetry. This may be more easily understood by a spatial rearrangement of the junctional resistances as shown in Fig. 16. Since each cell is assumed to have identical membrane components, we may for the moment omit them from consideration. The structure of Fig. 16 is a regular tetrahedron in which the path between any two cells is identical. Thus, into whichever cell the current is injected, the resultant voltages in the other three cells must be equal to each other although different from that in the injected cell. If the three coupled cells have identi-

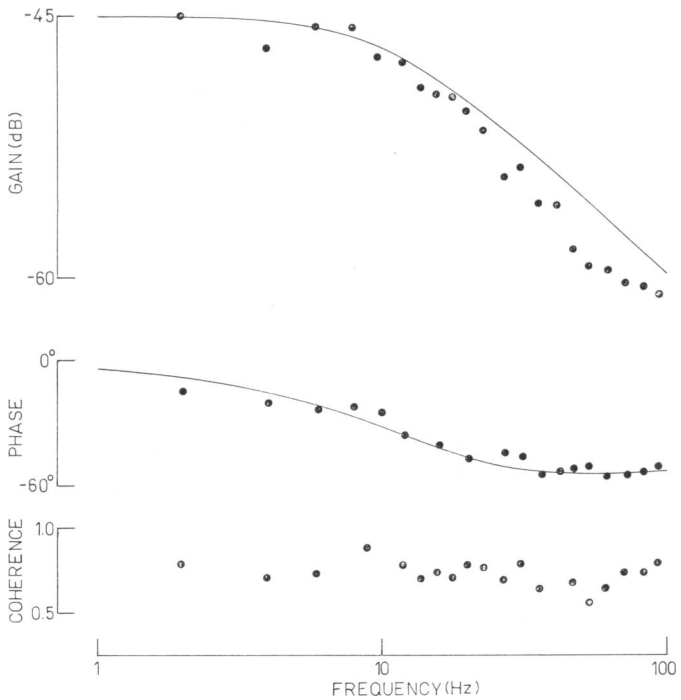

FIGURE 12 Frequency response and coherence functions between input and cell 1 for the four-cell embryo used in Fig. 11. Filled circles are experimental results and solid lines are theoretical predictions based upon the network of Fig. 13.

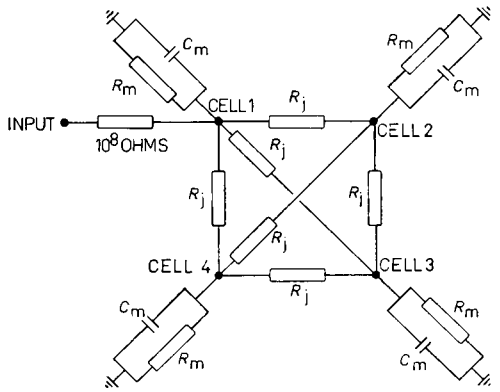

FIGURE 13 The simplest electrical network capable of explaining the behavior of a four-cell embryo. R_m and C_m are the plasma membrane resistances and capacitances and R_j are the intercellular junctional resistances.

tical voltages, then there can be no current flowing between them, and we may ignore all of the components which would carry current betweeen them. Referring to Fig. 13, this means that we may, for the purpose of analysis, ignore the junctional resistances between: cell 2-cell 3, cell 3-cell 4, and cell 2-cell 4; leaving three

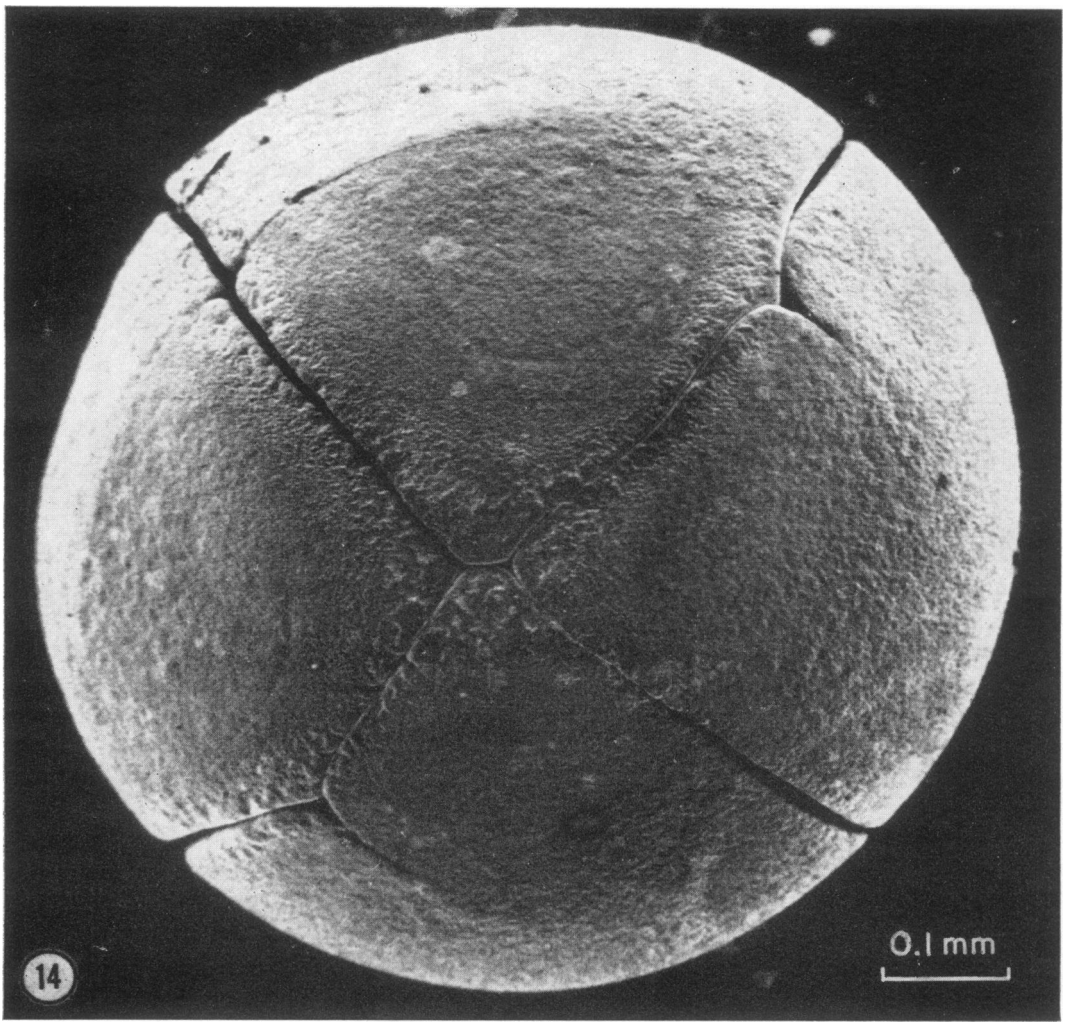

FIGURE 14 Scanning electron micrograph of the animal pole of a four-cell embryo. Note the area of close apposition of two diagonally opposite cells which causes separation of the other diagonal pair.

identical independent paths for the current to follow from cell 1, each consisting of R_j in series with the cell membrane components, C_m and R_m. Thus, we are dealing with a system which behaves as three individual two-cell systems sharing a common cell 1. For the steady current analysis we define the apparent lumped input resistance of cell 1 as R_L. Then:

$$R_L = [R_m(R_m + R_j)]/(4R_m + R_j), \quad (16)$$

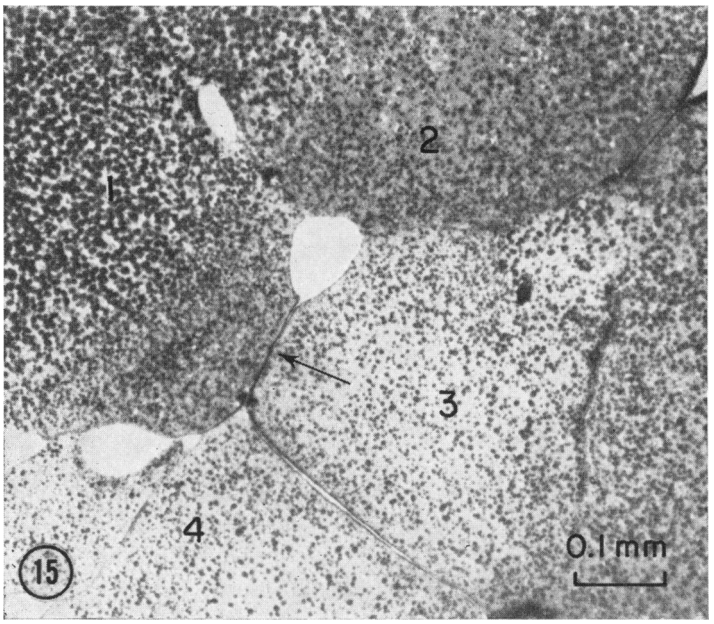

FIGURE 15 Light micrograph of a section through the vegetal hemisphere of a four-cell embryo. The cells are numbered 1–4. Close apposition of one pair of diagonal cells is indicated by the arrow.

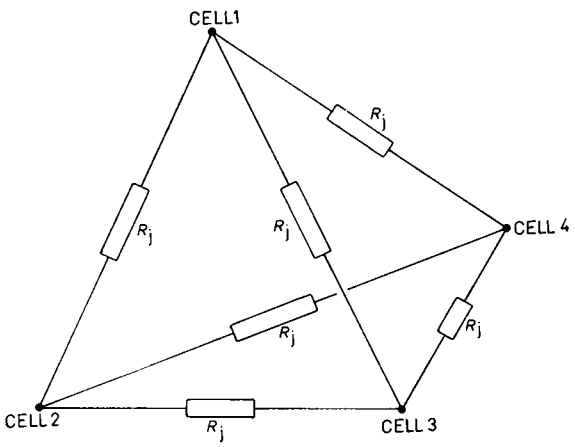

FIGURE 16 Perspective view of the six junctional resistances of Fig. 12 arranged in the form of a regular tetrahedron. In this spatial arrangement it is clear that the cells are electrically identical with each cell connected to all of its neighbors.

so that:

$$V_1/V_i = R_L/(R_L + 10^8). \tag{17}$$

We also have the coupling ratio:

$$CR = V_2/V_1 = V_3/V_1 = V_4/V_1 = R_m/(R_m + R_j). \tag{18}$$

Substituting Eq. 18 into Eq. 15 and solving for R_m, we obtain:

$$R_m = R_L + 3CR \cdot R_L, \tag{19}$$

and since R_L may be obtained directly from Eq. 17, R_m may be computed. R_j is then computed from Eq. 16 or Eq. 18. The value of C_m may be deduced from R_m, R_j and the cell-to-cell gain corner frequency, f_c, in a manner identical to that used for the two-cell case. For the embryo used in Figs. 11 and 12, we calculated values of $R_m = 2.10 \times 10^6\ \Omega$, $R_j = 4.18 \times 10^5\ \Omega$ and, $C_m = 0.0057\ \mu F$. These values were inserted into a modeled network of Fig. 13 and the frequency response functions corresponding to those of Figs. 11 and 12 were calculated using the ECAP program. A similar procedure was followed for the embryo of Fig. 10 using the calculated values of $R_m = 1.52 \times 10^6\ \Omega$, $R_j = 5.02 \times 10^5\ \Omega$, and $C_m = 0.0076\ \mu F$. The computed results are superimposed on the data in Figs. 10–12 as solid lines. The agreement between the frequency response functions of the experimental and modeled systems indicates that the circuit of Fig. 13 is an excellent model to account for the electrical behaviour of the four-cell embryo over the frequency range which we have used.

TABLE I

SUMMARY OF CALCULATED MEMBRANE PARAMETERS FOR TWO-CELL AND FOUR-CELL EMBRYOS

Where applicable the figures are expressed as the mean value ± the standard deviation. The maximum variation in embryonic diameter was less than 3% of the mean value so that the accuracies of the specific membrane properties are similar to the whole membrane measurements from which they were derived.

	First cleavage stage (2 cells)	Second cleavage stage (4 cells)	Units
Membrane potential	15.5±1.6	16.0±2.4	mV
Diameter of embryo	1.28	1.28	mm
Coupling ratio	0.772±0.058	0.808±0.026	
Membrane resistance (R_m)	1.05±0.16	1.80±0.20	MΩ
Specific membrane resistance	0.041	0.046	MΩcm²
Membrane capacitance (C_m)	0.0239±0.0035	0.0106±0.0047	μF
Specific membrane capacitance	0.62	0.41	μF/cm²
Junctional resistance (R_j)	0.286±0.071	0.421±0.061	MΩ
Membrane time constant	25	19	ms
Number of experiments	9	10	

In order to obtain specific membrane electrical characteristics, we measured the physical dimensions of embryos during the first two cleavage stages. Embryonic diameters were all within the range 1.25–1.31 mm and the mean value of 1.28 mm was used in all computations. Table I shows a summary of the membrane resistance, membrane capacitance, and junctional resistances which we measured for two- and four-cell embryos. In addition, we show the specific membrane resistances and specific membrane capacitances calculated from the assumption that the embryos are perfectly spherical and that the two- and four-cell stages contain perfect hemispherical and quarter-spherical cells, respectively.

DISCUSSION

General Membrane Properties

The membrane potentials which we have observed agree well with those reported for *Xenopus* by other workers (Palmer and Slack, 1970; de Laat et al., 1973), although the apparent plateau in potential during the two- and four-cell stages has not been demonstrated so clearly before. The reason for the rise in membrane potential from the very low value in single cell embryos is not clear. It is clearly not due to simple membrane leakage since the membrane becomes much more conductive after the single cell stage (Palmer and Slack, 1970).

The present results indicate that the specific cell membrane resistance remains fairly constant in the two- and four-cell stages. Palmer and Slack (1970) found a significant decrease in membrane resistance during the course of the second cleavage. However, their measurements were of total apparent cell membrane resistance, which is not a good estimator of the specific membrane resistance in a coupled system.

The Nature of Embryonic Electrotonic Coupling

As pointed out in the Introduction we are assuming that each of the nodes in our electrical network is known and that its voltage can be measured. The most obvious doubt in this assumption concerns the structure of the junctions. Some ultrastructural data is available on the contacts between *Xenopus* embryo cells during cleavage (Sanders and Zalik, 1972; Singal and Sanders, 1974). These studies have demonstrated the presence of point contacts possessing an intercellular gap of 20–30 Å. Such contacts provide a probable morphological basis for the coupling described in the present report since they are the only intimate cell contacts observed at the two- and four-cell stages. Similar intercellular junctions have been associated with electrotonic coupling in other systems (Payton et al., 1969; Gilula et al., 1972). No distinction was made between the ultrastructural contacts of adjacent cells and diagonal cells.

A detailed structural model of electrotonic junctions between cells has been

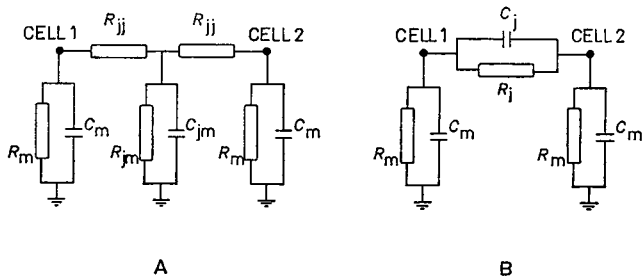

FIGURE 17 Two alternative hypothetical models for the two-cell embryo. In *A*, the junctional system is modeled by a "T" network of resistances, R_{jj} and R_{jm}, with a junctional membrane capacitance, C_{jm}. This arrangement would be expected if the junction behaves as a membranous cable. In *B*, a direct junctional capacitance, C_j, might be produced by the close apposition of the cell membranes in the junctional region.

proposed by McNutt and Weinstein (1970) in which relatively large membrane areas are apposed, with a closely packed two-dimensional array of subunits within the membranes and a hydrophilic channel passing through each subunit. With this in mind we shall consider two possible alternative circuits for the two-cell system as illustrated in Fig. 17.

Fig. 17 *A* is a model in which an additional resistance and capacitance are included to account for a cable-like structure between the cells. In the subunit array model the membrane surface area of the hydrophilic channels could be two small to produce any measurable conductance or capacitance. From the present results we can certainly say that the junctional membrane capacity, C_{jm}, must be very small relative to the other capacitances in the system since it would contribute another time constant to the circuit and produce different frequency response functions to those which we have measured. We cannot decide against the junctional membrane to ground resistance, R_{jm}, on the basis of our results since it would not change the type of frequency responses expected from the system. We can only say that it is unnecessary to invoke this resistance to explain the behavior of the system.

The other component whose presence may be conjectured on the basis of morphology is a direct junctional capacitance, C_j, as illustrated in Fig. 17 *B*. Such a capacitance might be expected in view of the close apposition of cell membranes which is believed to accompany intercellular coupling. However, the presence of a capacitance comparable to the cell membrane capacitance would clearly introduce another time constant into the circuit which would tend to produce a positive slope in the high frequency gain asymptote of the cell-to-cell frequency response function. C_j must be small enough to be undetectable by our present techniques.

Although it is possible to predict the electrical properties of a junctional system, given some physical model of the junctions, it is impossible to formulate a physical structure solely from electrical properties. This problem defines the primary limitation of electrical measurements; they are an excellent test of the feasibility of a

model for the system but are a poor predictor for an unknown structure. We must be content to say that any physical model for the mechanism of electrotonic coupling in *Xenopus* embryos must be compatible with the electrical properties which we have measured. One interesting property of electrotonic coupling, which may be deduced from our results, concerns the area of cell membrane associated with a given junctional conductance. It is not known, for example, whether the junctions between cells are few in number, localized, and of very high permeability, or whether there are relatively large numbers of junctions, of lower permeability, spread uniformly over the apposed membranes. Our finding, that all of the junctional resistances, R_j, in the four-cell embryo are identical, must be considered together with the fact that there is a much larger area of contact between adjacent cells than between diagonally opposite cells. This evidence suggests that junctional conductance is relatively independent of the area of closely apposed nonjunctional membrane and thus supports similar results obtained by Ito and Loewenstein (1969) for *Triturus* embryos. This is further illustrated by cases of electrotonic coupling between neurons, where cells are believed to have a very small area of mutual contact and yet display significant coupling coefficients (for example see Hagiwara and Morita, 1962).

The Developmental Significance of Electrotonic Coupling

It has been speculated that electrotonic coupling plays some, as yet unknown, role in the development of an embryo (Loewenstein, 1968 *a*). Our findings in the case of the four-cell embryo appear relevant to this speculation since if our results have been interpreted correctly, then the four-cell embryo is equipped to have electrotonic coupling between its cells such that each is identically linked to each of its fellows. It is important to note that the coupling ratio between adjacent cells in a four-cell embryo is sufficiently high that diagonally opposed cells would be coupled almost as closely to each other anyway, via their adjacent cells, as they are by their specific coupling resistances. Again, the relatively small areas of contact between diagonally opposed cells appear to be sites of the same junctional current carrying capacity as the much larger areas of contact between adjacent cells. It is difficult to suppose that there is not some functional significance in this arrangement which keeps the cells in such intimate electrical contact.

A further consideration is that during the two- and four-cell stages the cells are not all qualitatively similar. The area known as the grey crescent is not uniformly present on all cells during these stages. Our finding that all of the cells are equally coupled assumes some importance in view of the demonstration by Curtis (1962) that the grey crescent is of morphogenetic significance prior to the eight-cell stage. If material is diffusing from the crescent region to all of the cells via intercellular junctions then complete direct coupling throughout the embryo may be valuable. Curtis (1962) has found that the embryonic cells become unresponsive to the

influence of the grey crescent at the eight-cell stage and we are currently determining whether there is a corresponding change in intercellular coupling at this stage. It has been demonstrated by means of fluorescent dye injection that molecules having a molecular weight of at least 330 are able to pass between coupled embryonic cells (Sheridan, 1971). Soon after the four-cell stage a system must be established in which much intercellular coupling is via intervening cells since there is no morphological evidence for the large number of intercellular cytoplasmic processes which direct coupling would necessitate. If direct cell-to-cell coupling is important up to the four-cell stage, this might be correlated with different developmental potencies of these cells compared to those of more advanced stages. We hope to address ourselves to this question in future work.

Support for this work was provided by the Medical Research Council of Canada through operating grants to A. S. French and E. J. Sanders and through the provision of a studentship to R. A. DiCaprio.

Received for publication 30 October 1973.

REFERENCES

ASHMAN, R. F., Y. KANNO, and W. R. LOEWENSTEIN. 1964. *Science (Wash. D. C.).* **145**:604.
BENDAT, J. S., and A. G. PIERSOL. 1966. Measurement and Analysis of Random Data. John Wiley & Sons, Inc., New York.
BENNETT, M. V. L., M. E. SPIRA, and G. D. PAPPAS. 1972. *Dev. Biol.* **29**:419.
BENNETT, M. V. L. and J. P. TRINKAUS. 1970. *J. Cell Biol.* **44**:592.
BLUEMINK, J. G. 1971. *Cytobiologie.* **3**:176.
BLUEMINK, J. G. 1972. *J. Ultrastruct. Res.* **41**:95.
BOZHKOVA, V. P., S. A. KOVALEV, L. M. CHAILAKHYAN, and E. N. SHILYANSKAYA. 1971. *Ontogenez.* **2**:512.
COOLEY, J. W., and J. W. TUKEY. 1965. *Math. Comput.* **19**:297.
CURTIS, A. S. G. 1962. *J. Embryol. Exp. Morphol.* **10**:410.
DAWID, I. B. 1965. *J. Mol. Biol.* **12**:581.
D'AZZO, J. J., and C. H. HOUPIS. 1966. Feedback Control System Analysis and Synthesis. McGraw-Hill, Inc., New York.
DE LAAT, S. W., D. LUCHTEL, and J. G. BLUEMINK. 1973. *Dev. Biol.* **31**:163.
FRENCH, A. S. 1973 *a. Comput. Programs Biomed.* **3**:45.
FRENCH, A. S. 1973 *b. IEEE Trans. Bio-Med. Eng.* In press.
FRENCH, A. S. and A. V. HOLDEN. 1971. *Comput. Programs Biomed.* **1**:219.
FURSHPAN, E. J., and D. D. POTTER. 1968. *Curr. Top. Dev. Biol.* **3**:95.
GILULA, N. B., O. R. REEVES, and A. STEINBACH. 1972. *Nature (Lond.).* **235**:262.
HAGIWARA, S., and H. MORITA. 1962. *J. Neurophysiol.* **25**:721.
HAMBURGER, V. 1960. A Manual of Experimental Embryology. University of Chicago Press, Chicago, Ill.
ITO, S., and N. HORI. 1966. *J. Gen. Physiol.* **49**:1019.
ITO, S., and W. R. LOEWENSTEIN. 1969. *Dev. Biol.* **19**:228.
LOEWENSTEIN, W. R. 1966. *Ann. N. Y. Acad. Sci.* **137**:441.
LOEWENSTEIN, W. R. 1967. *Dev. Biol.* **15**:503.
LOEWENSTEIN, W. R. 1968 *a. Perspect. Biol. Med.* **11**:260.
LOEWENSTEIN, W. R. 1968 *b. Dev. Biol. Suppl.* **2**:151.
MCNUTT, N. S., and R. S. WEINSTEIN. 1970. *J. Cell Biol.* **47**:666.
OLIVEIRA-CASTRO, G. M., and W. R. LOEWENSTEIN. 1971. *J. Membrane Biol.* **5**:51.

PALMER, J. F., and C. SLACK. 1970. *J. Embryol. Exp. Morphol.* **24**:535.
PAYTON, B. W., M. V. L. BENNETT, and G. D. PAPPAS. 1969. *Science (Wash. D. C.).* **166**:1641.
POTTER, D. D., E. J. FURSHPAN, and E. S. LENNOX. 1966. *Proc. Natl. Acad. Sci. U.S.A.* **55**:328.
ROSE, B. 1971. *J. Membrane Biol.* **5**:1.
SALTHE, S. M. 1963. *J. Morphol.* **113**:161.
SANDERS, E. J., and P. K. SINGAL. 1973. *Micron.* **4**:156.
SANDERS, E. J., and S. E. ZALIK. 1972. *Wilhelm Roux' Arch. Entwicklungsmech. Org.* **171**:181.
SHERIDAN, J. D. 1968. *J. Cell Biol.* **37**:650.
SHERIDAN, J. D. 1971. *Dev. Biol.* **26**:627.
SINGAL, P. K., and E. J. SANDERS. 1974. *J. Ultrastruct. Res.* In press.
SLACK, C., and J. F. PALMER. 1969. *Exp. Cell Res.* **55**:416.
TAKAHASHI, M., and S. ITO. 1968. *Zool. Mag.* **77**:307.
TUPPER, J., J. W. SAUNDERS, and C. EDWARDS. 1970. *J. Cell Biol.* **46**:187.
TUPPER, J., and J. W. SAUNDERS. 1972. *Dev. Biol.* **27**:546.
WIENER, N. 1930. *Acta Math.* **55**:117.